Electronic Supplementary Material (ESI) for Physical Chemistry Chemical Physics.

Establishing the pivotal role of local aromaticity in the electronic properties of graphene lateral hybrids

Nicolás Otero[*][†], Khaled E. El-kelany[*][‡], Michel Rérat[*], Claude Pouchan[*] and Panaghiotis Karamanis[*]

---

[*] Équipe de Chimie Théorique, ECP Institut des Sciences Analytiques et de Physico-chimie pour l'Environnement et les Materiaux (IPREM) UMR 5254, Hélioparc Pau Pyrénées 2 avenue du President Angot, 64053 Pau Cedex 09, France

[†] Departamento de Química Física, Universidade de Vigo, 36310 Vigo, Galicia, Spain

[‡] CompChem Lab, Chemistry Department, Faculty of Science, Minia University, Minia 61519 Egypt

1 Results and discussion

The aim of this section is to glimpse the effect of the carbon aromaticity patterns of two molecular systems embedded in a hexagonal BN slab, called C_{84} and hexa-peri-hexabenzocoronene (HBC), on a confined borazine ring by considering both periodic and finite systems through the analysis of total and Mulliken-based projected density of states (DOS) spectra. Firstly, we have examined the considered periodic systems in order to indicate the representative variations when the central benzene ring is replaced by the corresponding B−N borazine ring. Next, we have studied the isolated carbon structures to see where the last occupied and first virtual orbitals levels come from, and, finally, these systems have been embedded into finite h-BN slabs to verify that the same patterns are preserved.

We have obtained two trends through periodic calculations (Figure 1), computed by the CRYSTAL14 program[1] at LDA/6-31G* level of calculation controlled by a shrinking factor of (2,2,0) corresponding to 3 k-points and the Coulomb and exchange truncation tolerances of (6,6,6,6,12). Noteworthily, this low number of k-points used in the reciprocal space necessary to model the HOMO-LUMO gap seems to be adequate since the increase of the k-points entails no energetic changes of the gap, confirmed by an invariable energy involved in the levels around the HOMO-LUMO gap (Figure 2). In fact, it is reasonable to think that a finite model could provide the same description and, in addition, simplifying the model. This idea is newly brought to light in view of the fact the green peaks of the projected DOS contributions concerning the embedded structures form the majority of the total DOS peaks, as was zoomed in Figures 1a and 1b. This emphasizes the local dependence of the gap with respect to the enclosed structure and, therefore, the unnecessary use of DOS plots to study the HOMO-LUMO region through periodic models.

Nonetheless, despite the DOS spectra are a valuable tool to study the electronic bands structure of solids, they are unrigorously defined in finite systems due to the artificial extension of the discrete energy levels and the sum performed over them. In contrast, they provide a fast and comprehensive perspective to analyze the importance and ordering of the complete or partial set of molecular orbitals, especially surrounding the HOMO and LUMO. Among several line broadening mechanisms that can be found, we have chosen the gaussian expansion of the discrete energy levels through a width parameter of 0.136 eV applied to C_{84} and HBC structures embedded in a hexagonal BN slab and isolated to indicate the variations when the central benzene ring is replaced by the corresponding B$-$N borazine ring. Notice that the electron delocalization and connectivity linked to the aromaticity of the HBC and C_{84} provoke different effects on the rings, i.e., the HBC aromatic rings present larger delocalization, increasing the HOMO-LUMO gap, in comparison with a slighter effect of C_{84}-based structures. Moreover, the central ring is aromatic and nonaromatic for the HBC and C_{84} systems, respectively, provoking a different trend on the behavior of the molecules when it is replaced, as can be observed in Figures 3a and 3b. All calculations based on finite structures were performed by means of Multiwfn program[2] through the calculation and analysis of the DOS implemented there.

Notice that the electron delocalization and connectivity linked to the aromaticity of the HBC and C_{84} provoke different effects on the rings, i.e., the HBC aromatic rings present larger delocalization, increasing the HOMO-LUMO gap, in comparison with a slighter effect of C_{84}-based structures. Moreover, the central ring is aromatic and nonaromatic for the HBC and C_{84} systems, respectively, provoking a different trend on the behavior of the molecules when it is replaced, as can be observed in Figures 3a and 3b. All calculations based on finite structures were performed by means of Multiwfn program[2] through the calculation and analysis of the DOS implemented there.

For the sake of comparison, we have employed in our projected DOS spectra three alternated carbons from the central ring to compare them with the three boron and three nitrogen homologous of the B_3N_3 ring surrounding the HOMO-LUMO levels. Besides, we have marked the key peaks involved in the process, four and two for C_{84} and HBC spectra, respectively. In the case of the former molecule, two kinds of situations are represented by the plots in Figure 3c. On the one hand, the corresponding values from the central nonaromatic ring at -4.86 eV (peak B) and -2.79 eV (peak C), whose estimation of density of states is relatively low in comparison with, on the other hand, the corresponding peaks A and D formed from the aromatic rings in contact with these carbon atoms. Nonetheless, the former peaks (B and C) disappear for the HBC structure (Figure 3d), since they are combined with other close levels such as peaks A' and D' at -5.24 eV and -2.23 eV. In fact, these peaks are respectively destabilized and stabilized in comparison with those from the molecule called C_{84}.

Concerning the BN-doped structures, the spectra are clearly altered by the replacement of the central ring by its isoelectronic counterpart, that is, the HOMO-LUMO gap is modified as was previously described in the main body of the article and observed in Figures 4a and 4b. Once more, one can observe the same four peaks scheme around the HOMO-LUMO region in the $C_{84}-B_3N_3$ (Figure 4c). However, the DOSs are larger for the corresponding HOMO and LUMO peaks in both structures. In addition, the atomic decomposition of the total DOS plots indicate that these levels are predominantly controlled by different elements, that is, while the B atoms rule the HOMO level in the case of the $C_{84}-B_3N_3$ molecule, the nitrogens are the ones controlling the LUMO, and, regarding the $HBC-B_3N_3$ structure, the effect is inversely ruled. Bear in mind that this reversal comes from replacing a ring that would correspond to an aromatic ring in the pure flake by a nonaromatic one created from the electronegativity difference between B and N atoms. Therefore, the connectivity and delocalization of the rest of the molecule, i.e., the aromaticity pattern of the system, will provoke different behavior on the hexagonal BN ring, but in a similar way in comparison with the pure structures. This is the main reason why a similar scheme is kept in the projected DOS spectra (Figures 3c and 3d).

The peaks A/D and A'/D' can be seen as common points in both situations, despite being slightly shifted in the case of the HBC-based structures. For instance, the levels at $-6.02\,\mathrm{eV}$ (peak A) and $-1.64\,\mathrm{eV}$ (peak D) in the $C_{84}-B_3N_3$ flake, match with those at $-5.46\,\mathrm{eV}$ (peak A') and $-1.91\,\mathrm{eV}$ (peak D') levels. When the central ring substitution is performed on the HBC, a large contribution of the electrons that were defined in the $C_{84}-B_3N_3$ HOMO from the boron atoms are destabilized to become part of the LUMO while the level at $-2.94\,\mathrm{eV}$ (peak C) would be transferred to the $HBC-B_3N_3$ HOMO (peak A'), since these peaks disappear and the larger ones are slightly shifted, increasing, besides, the density of states of peaks A' and D'. The possible hint of this "π stabilization" of the N atoms is the increase of Mulliken π populations (Table 1), in view of the decrease in energy of the virtual $C_{84}-B_3N_3$ nitrogen LUMO level transferred to the HOMO orbital and, therefore, triggering the increase of the populations.

$C_{84}-B_3N_3$ and HBC$-B_3N_3$ molecules were embedded into periodic hexagonal BN 2D systems, obtaining the same trend (Figures 5 to 7 and 9 to 11). Similarly, Figures 5a, 5b, 6a, 6b, 7a and 7b show the complete (black line) and only including the embedded structure (green line) DOS plots of the BN13 × 13$-C_{84}-B_3N_3$ and BN13 × 13$-$HBC$-B_3N_3$ passivated finite unit cells, also marking the HOMO as a dashed line. As can be seen, the predominant atoms for the levels around the HOMO and LUMO clearly come close to the embedded structure in both cases. This definitely means the C_{84} and HBC lead any process related to the HOMO-LUMO gap and, therefore, to the stabilization of the overall systems. As is expected in view of the aromaticity pattern and our delocalization indices, the HBC structure is more stable and, in consequence, more aromatic, since the HOMO-LUMO gap is larger than that corresponding to the another one. When the B_3N_3 central ring is specifically taken into account (Figures 5c and 5d), one can observe the different effect of the aromaticity patterns on this fragment. The peaks A/A' and D/D' can be considered kept around the HOMO in both structures and, due to the environment variation (different aromaticity pattern), the sum of DOS is modified, provoking the consequent different peaks around the HOMO-LUMO region. Concerning the central nitrogens, the main difference between the two embedded structures is mainly the stabilization of the contribution at $-3.92\,\mathrm{eV}$ value (peak D) and, especially, at $-4.89\,\mathrm{eV}$ (peak C) to become the HOMO level at $-7.02\,\mathrm{eV}$ value (peak A').

Finally, the basis set modifications keep the previously indicated trends, as can be shown in Figures 6, 7, 10 and 11. Moreover, as a matter of fact, our results show these trend variations between $C_{84}-B_3N_3$ and HBC$-B_3N_3$ are caused by different aromaticity patters. Furthermore, taking into account these kinds of structures are a type of polycyclic aromatic hydrocarbons (PAHs), their aromaticity behavior comes from the π orbitals. Therefore, whenever one considers the π symmetric basis functions, the spectra obtained around the HOMO and LUMO levels are completely equivalent compared with those including all basis functions (Figures 4c, 4d, 5c, 5d, 6c, 6d, 7c and 7d vs. Figures 8 to 11). All these aforesaid points clearly demonstrate that the confinement and modification of carbon-based fragments in both finite and periodic hexagonal B$-$N slabs provoke the same effects to the HOMO-LUMO gap and, for this reason, in the reactivity and several macroscopic properties of the whole system such as dipole (hyper)polarizabilities. Furthermore, these results demonstrate that while the aromaticity patterns are strong enough, as is the case of these nanoscaled embedded carbon structures, the HOMO-LUMO gap is ruled by the embedded structure, and any modification of the graphene section is affected by the aromaticity patterns. In contrast, the mechanism of stabilization/destabilization of the peaks are slightly different: the peaks B and C do not seem to be transferred (at least partially) to the peaks A' and D' as was mentioned above, keeping the same density of states.

In conclusion, when in a hexagonal BN periodic or finite system, an embedded structure formed by graphene-based nanostructures is introduced, the π aromaticity of this fragment rules the HOMO-LUMO gap. Hence, any perturbation of the corresponding electrons of this confined section will affect the highest occupied molecular orbitals, changing the final order and DOS of them. In fact, the same perturbation (e.g., the interaction or replacement of one/several atoms) in different places can induce completely opposite changes depending on whether the ring is aromatic or nonaromatic. Thus, when a nonaromatic (aromatic) ring is replaced by the BN counterpart, the influence from the borons (nitrogens) on the HOMO level prevails over the nitrogens (borons). In case one is replacing a nonaromatic ring of a pattern based on the C_{84} molecule, two levels of energy will be related to the aromaticity analogue pattern-based molecule, HBC, in addition to the HOMO and LUMO. These are the immediately closest ones, whose DOSs are higher, and play a crucial role, since they will become the new HOMO and LUMO levels. This is caused by the fact the aromaticity pattern stabilizes the nitrogens, while the borons become more unstable in view of our DOS plots. Proof of this stabilization and not an internal redistribution of the occupied orbitals is the systematic increase of the nitrogens π populations, since the virtual orbitals are unaccounted for the electron density.

Figure 1: Total and Mulliken-based projected DOS spectra calculated at LDA/6-31G* level of calculation (controlled by a shrinking factor of (2,2,0) corresponding to 3 k-points and the Coulomb and exchange truncation tolerances of (6,6,6,6,12)) of $C_{84}{-}B_3N_3$ and $HBC{-}B_3N_3$ embedded in a periodic hexagonal BN slab, where the central benzene ring was replaced by borazine. The projected DOS plots consider the embedded structures ((a) and (b)) and the borazine ring ((c) and (d)). The latter ones were scaled by a factor of 50.00. HOMO level is marked by a dashed line.

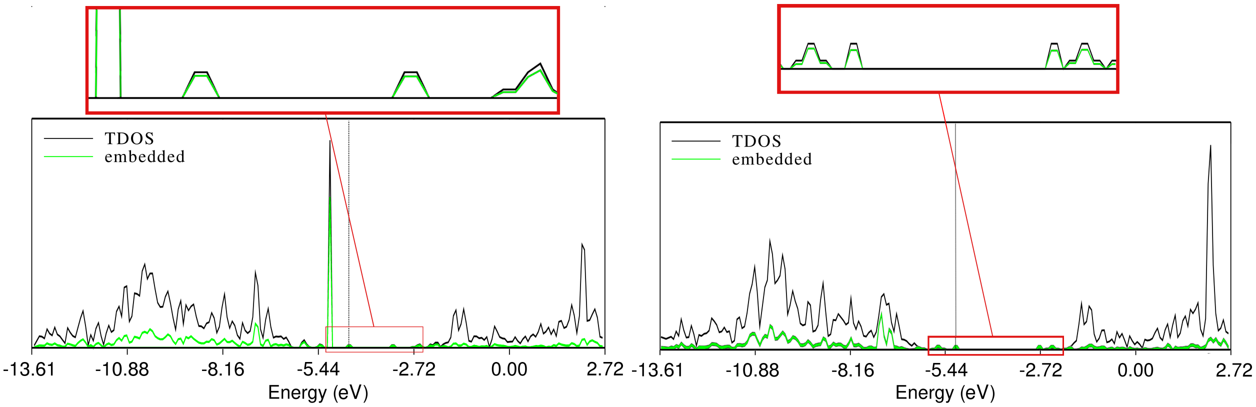

(a) BN13 × 13$-C_{84}-B_3N_3$ total+embedded

(b) BN13 × 13$-HBC-B_3N_3$ total+embedded

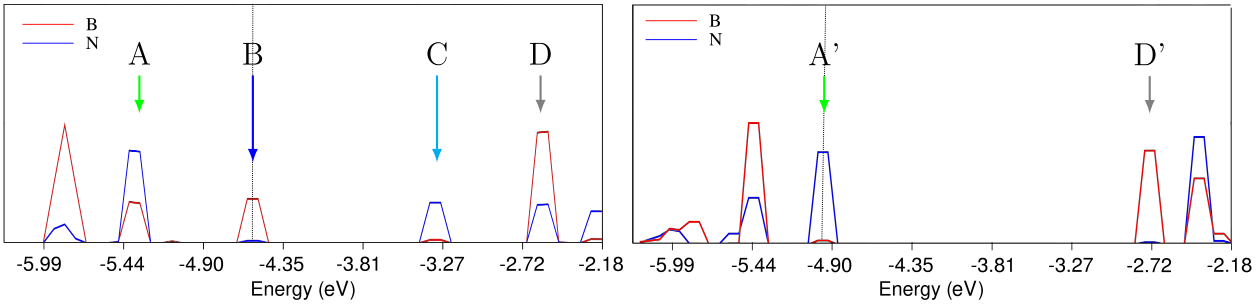

(c) BN13 × 13$-C_{84}-B_3N_3$ central ring

(d) BN13 × 13$-C_{84}-B_3N_3$ central ring

Figure 2: Band structures of $C_{84}-B_3N_3$ (a) and $HBC-B_3N_3$ (b) embedded in a periodic hexagonal BN slab, where the central benzene ring was replaced by borazine. The plots were computed at LDA/6-31G* level of calculation controlled by a shrinking factor of (2,2,0) corresponding to 3 k-points and the Coulomb and exchange truncation tolerances of (6,6,6,6,12). All values are in atomic units.

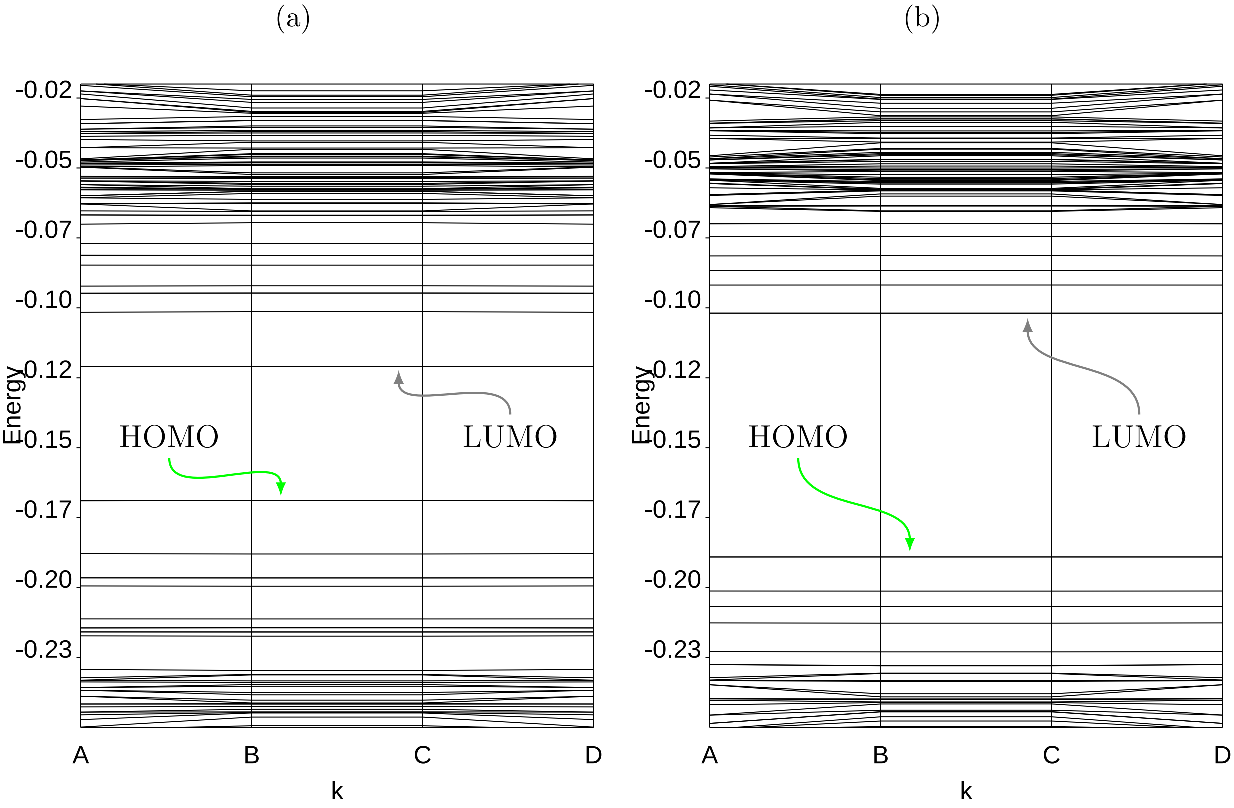

Figure 3: Total and Mulliken-based projected DOS spectra calculated at HSE06/6-31G//HSE06/MINI of C_{84} and HBC molecules. The projected DOS plots, which were scaled by a factor of 44.44, consider three alternated carbons of the central ring. HOMO level is marked by a dashed line in all spectra.

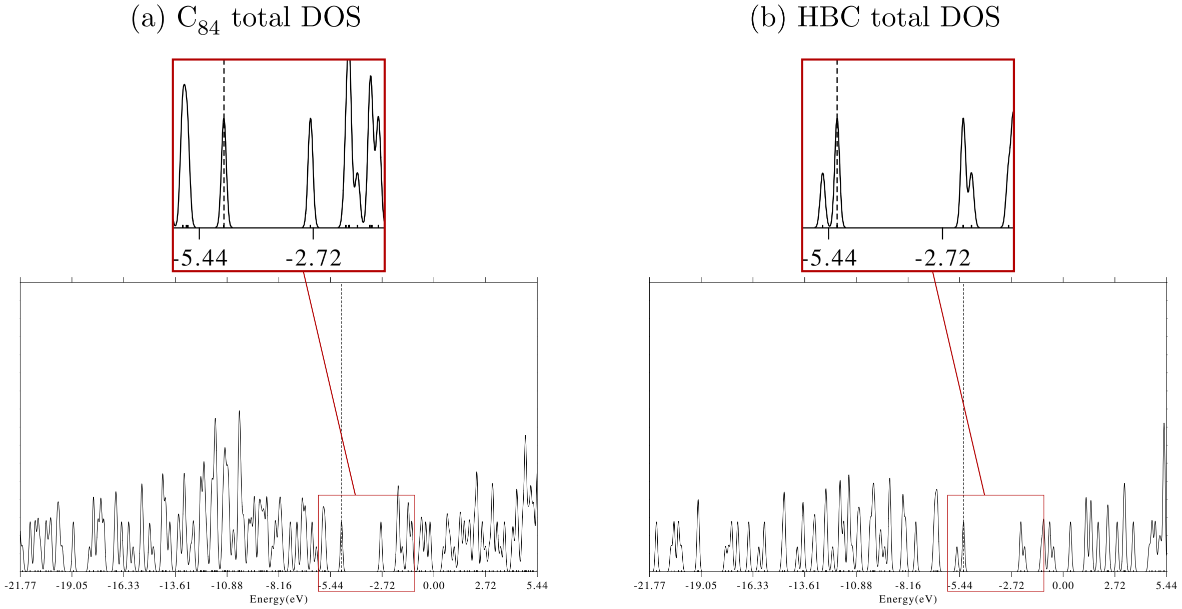
(a) C_{84} total DOS

(b) HBC total DOS

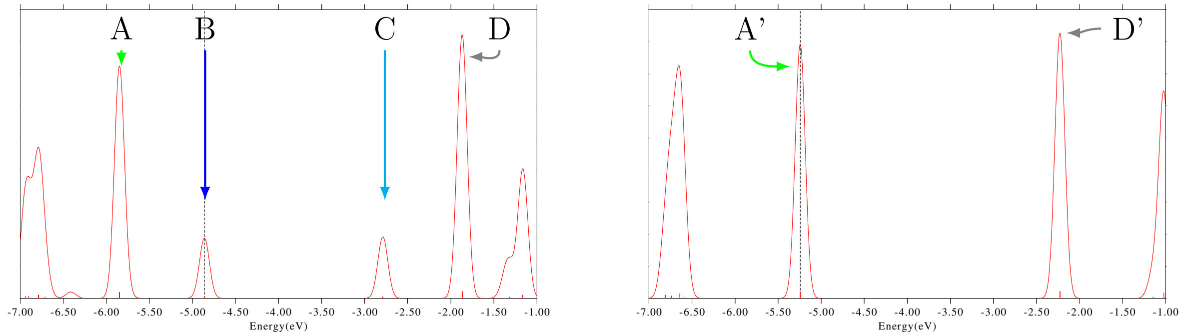
(c) C_{84} central ring projected DOS

(d) HBC central ring projected DOS

Figure 4: Total and Mulliken-based projected DOS spectra calculated at HSE06/6-31G//HSE06/MINI of $C_{84}-B_3N_3$ and $HBC-B_3N_3$, where the central benzene ring was replaced by borazine. The projected DOS plots, which were scaled by a factor of 44.44, consider this ring. HOMO level is marked by a dashed line.

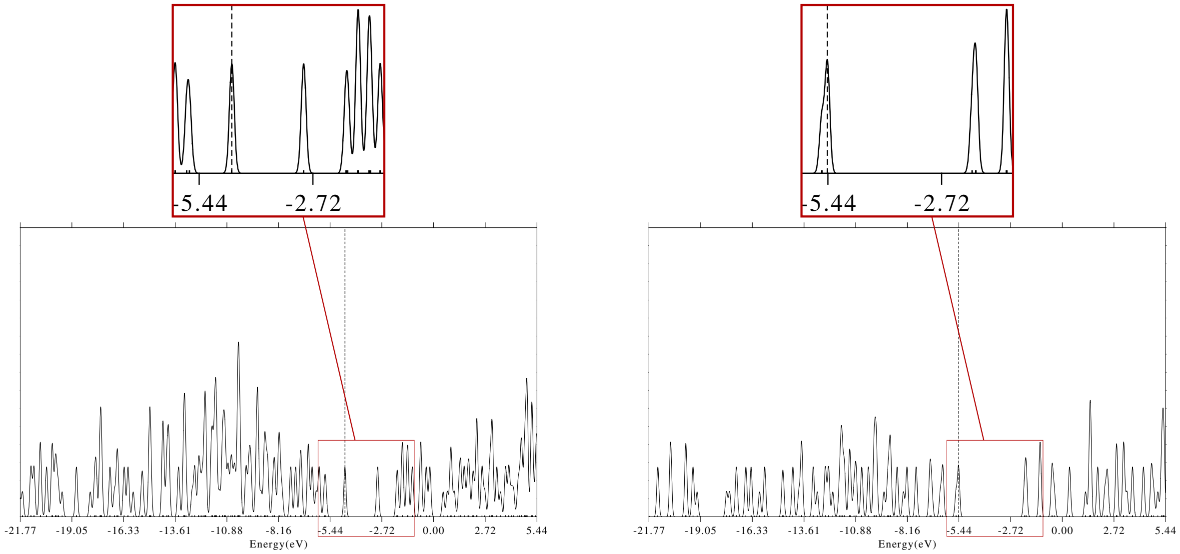

(a) $C_{84}-B_3N_3$ total DOS

(b) $HBC-B_3N_3$ total DOS

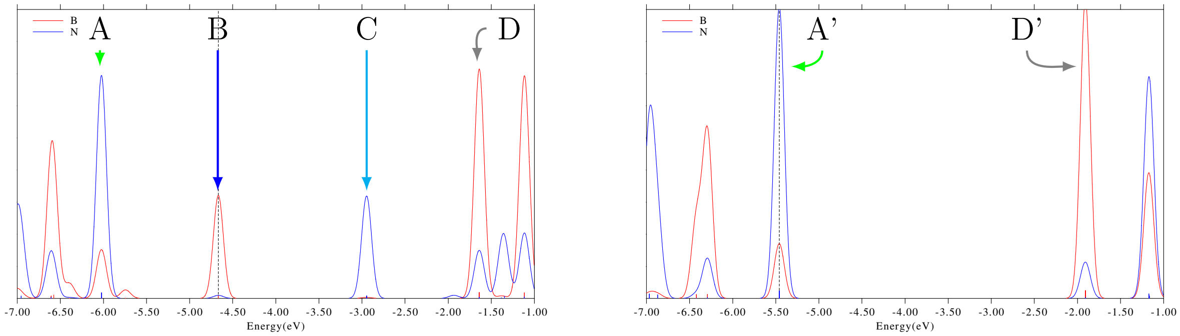

(c) $C_{84}-B_3N_3$ central ring projected DOS

(d) $HBC-B_3N_3$ central ring projected DOS

Figure 5: Total and Mulliken-based projected DOS spectra calculated at HSE06/MINI of BN13 × 13$-$C$_{84}$$-B_3N_3$ and BN13 × 13$-$HBC$-$B$_3$N$_3$, where the central benzene ring was replaced by borazine. The projected DOS plots consider the embedded structures ((a) and (b)) and the borazine ring ((c) and (d)). The latter ones were scaled by a factor of 50.00. HOMO level is marked by a dashed line.

(a) BN13 × 13$-$C$_{84}$$-B_3N_3$ total+embedded

(b) BN13 × 13$-$HBC$-$B$_3$N$_3$ total+embedded

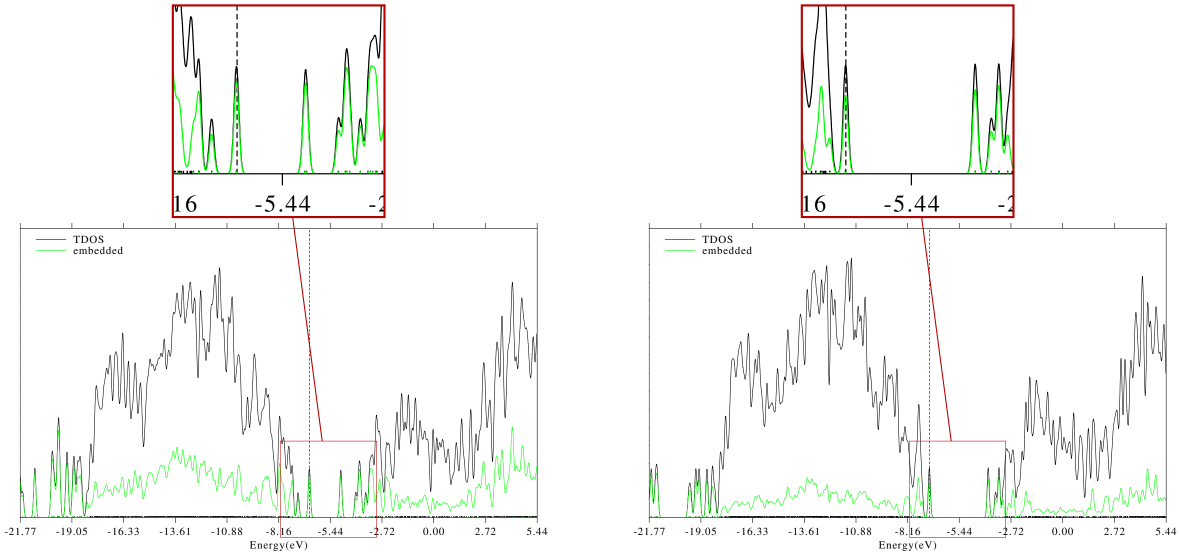

(c) BN13 × 13$-$C$_{84}$$-B_3N_3$ central ring

(d) BN13 × 13$-$HBC$-$B$_3$N$_3$ central ring

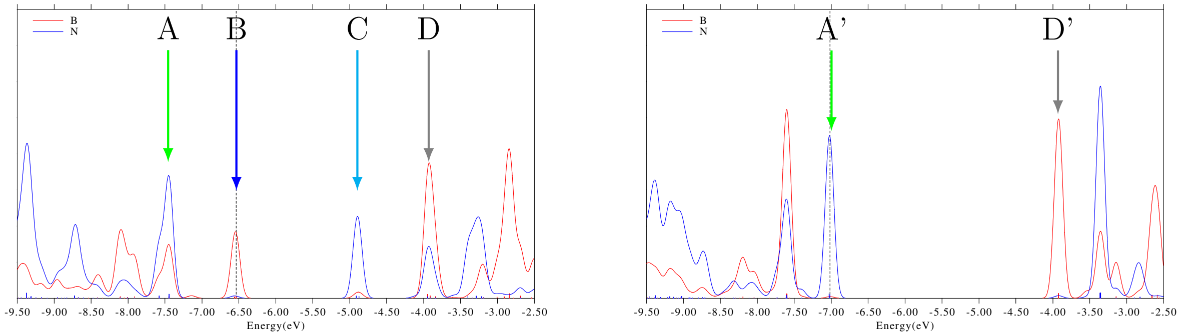

Figure 6: Total and Mulliken-based projected DOS spectra calculated at HSE06/6-31G//HSE06/MINI of BN13 × 13−C_{84}−B_3N_3 and BN13 × 13−HBC−B_3N_3, where the central benzene ring was replaced by borazine. The projected DOS plots consider the embedded structures ((a) and (b)) and the borazine ring ((c) and (d)). The latter ones were scaled by a factor of 50.00. HOMO level is marked by a dashed line.

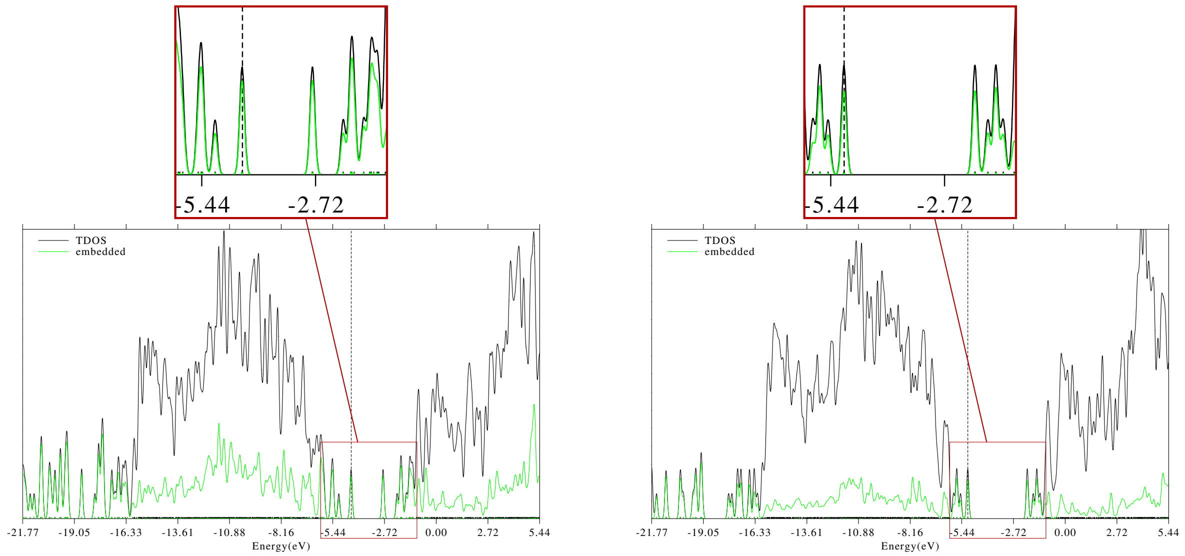

(a) BN13 × 13−C_{84}−B_3N_3 total+embedded

(b) BN13 × 13−HBC−B_3N_3 total+embedded

(c) BN13 × 13−C_{84}−B_3N_3 central ring

(d) BN13 × 13−HBC−B_3N_3 central ring

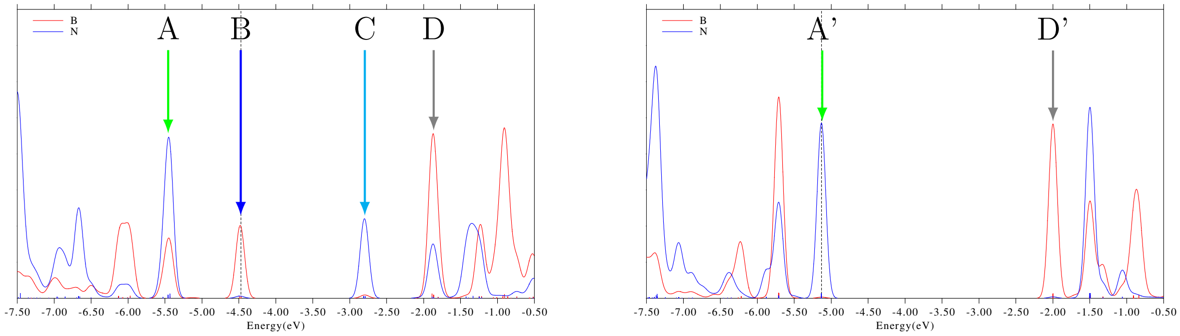

Figure 7: Total and Mulliken-based projected DOS spectra calculated at HSE06/6-31G*//HSE06/MINI of BN$13 \times 13-\mathrm{C}_{84}-\mathrm{B}_3\mathrm{N}_3$ and BN$13 \times 13-\mathrm{HBC}-\mathrm{B}_3\mathrm{N}_3$, where the central benzene ring was replaced by borazine. The projected DOS plots consider the embedded structures ((a) and (b)) and the borazine ring ((c) and (d)). The latter ones were scaled by a factor of 50.00. HOMO level is marked by a dashed line.

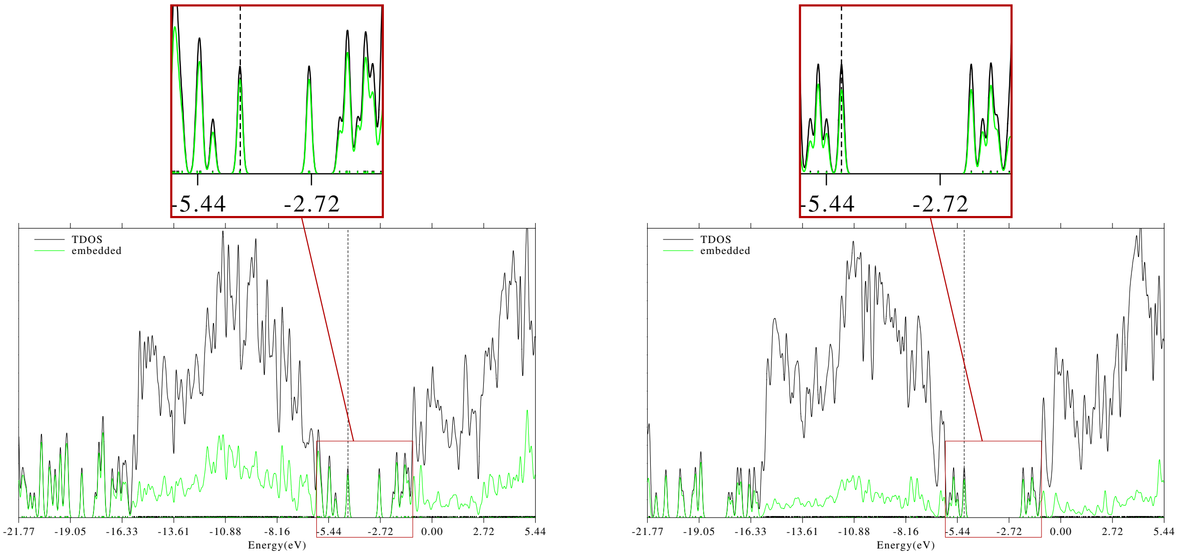

(a) BN$13 \times 13-\mathrm{C}_{84}-\mathrm{B}_3\mathrm{N}_3$ total+embedded

(b) BN$13 \times 13-\mathrm{HBC}-\mathrm{B}_3\mathrm{N}_3$ total+embedded

(c) BN$13 \times 13-\mathrm{C}_{84}-\mathrm{B}_3\mathrm{N}_3$ central ring

(d) BN$13 \times 13-\mathrm{HBC}-\mathrm{B}_3\mathrm{N}_3$ central ring

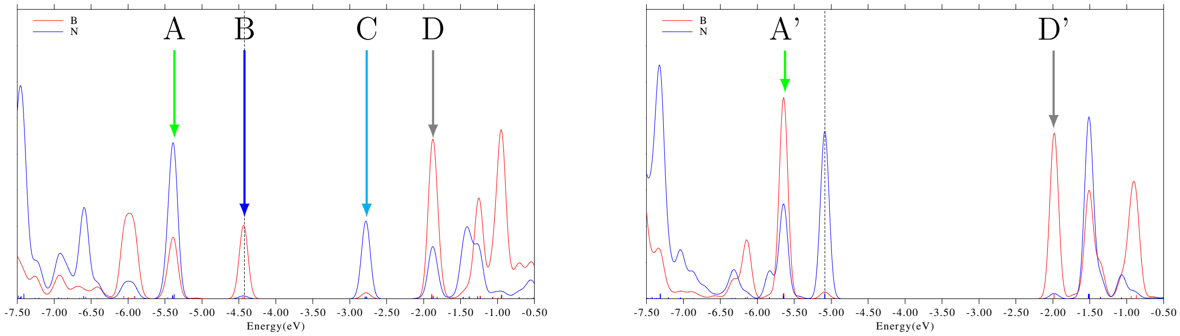

Figure 8: Mulliken-based projected DOS spectra calculated at HSE06/6-31G//HSE06/MINI of $C_{84}-B_3N_3$ and HBC$-B_3N_3$, where the central benzene ring was replaced by borazine. π-symmetric basis functions were only employed to obtain these plots scaled by a factor of 50.00. HOMO level is marked by a dashed line.

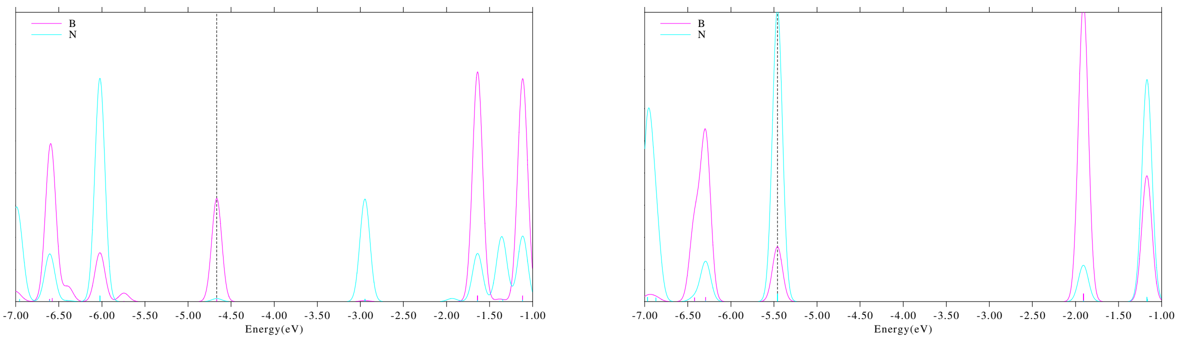

(a) BN13 × 13$-C_{84}-B_3N_3$ central ring

(b) BN13 × 13$-$HBC$-B_3N_3$ central ring

Figure 9: Mulliken-based projected DOS spectra calculated at HSE06/MINI of BN13 × 13$-C_{84}-B_3N_3$ and BN13 × 13$-$HBC$-B_3N_3$, where the central benzene ring was replaced by borazine. π-symmetric basis functions were only employed to obtain these plots scaled by a factor of 50.00. HOMO level is marked by a dashed line.

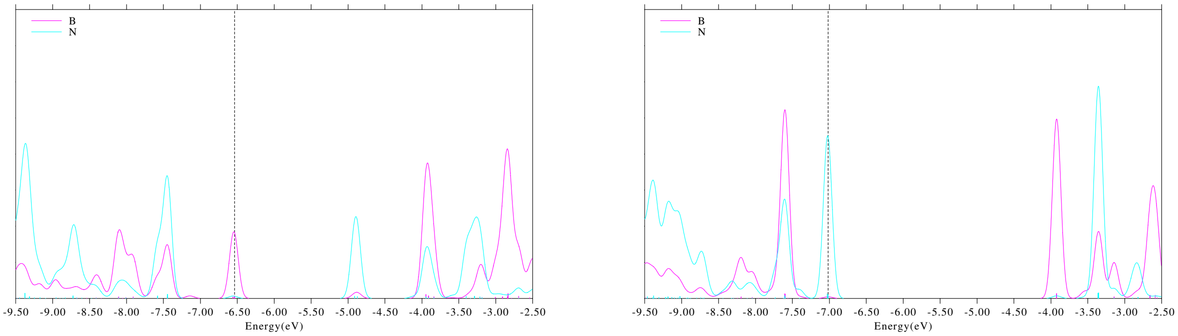

(a) BN13 × 13$-C_{84}-B_3N_3$ central ring

(b) BN13 × 13$-$HBC$-B_3N_3$ central ring

Figure 10: Mulliken-based projected DOS spectra calculated at HSE06/6-31G//HSE06/MINI of BN13 × 13$-$C$_{84}$$-B_3N_3$ and BN13 × 13$-$HBC$-$B$_3$N$_3$, where the central benzene ring was replaced by borazine. π-symmetric basis functions were only employed to obtain these plots scaled by a factor of 50.00. HOMO level is marked by a dashed line.

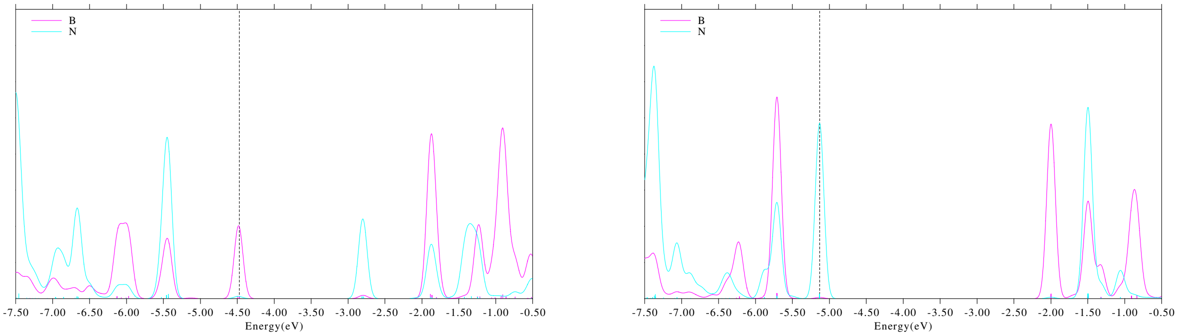

(a) BN13 × 13$-$C$_{84}$$-B_3N_3$ central ring

(b) BN13 × 13$-$HBC$-$B$_3$N$_3$

Figure 11: Mulliken-based projected DOS spectra calculated at HSE06/6-31G*//HSE06/MINI of $\mathrm{BN13}\times 13-\mathrm{C}_{84}-\mathrm{B}_3\mathrm{N}_3$ and $\mathrm{BN13}\times 13-\mathrm{HBC}-\mathrm{B}_3\mathrm{N}_3$, where the central benzene ring was replaced by borazine. π-symmetric basis functions were only employed to obtain these plots scaled by a factor of 50.00. HOMO level is marked by a dashed line.

(a) $\mathrm{BN13}\times 13-\mathrm{C}_{84}-\mathrm{B}_3\mathrm{N}_3$ central ring

(b) $\mathrm{BN13}\times 13-\mathrm{HBC}-\mathrm{B}_3\mathrm{N}_3$ central ring

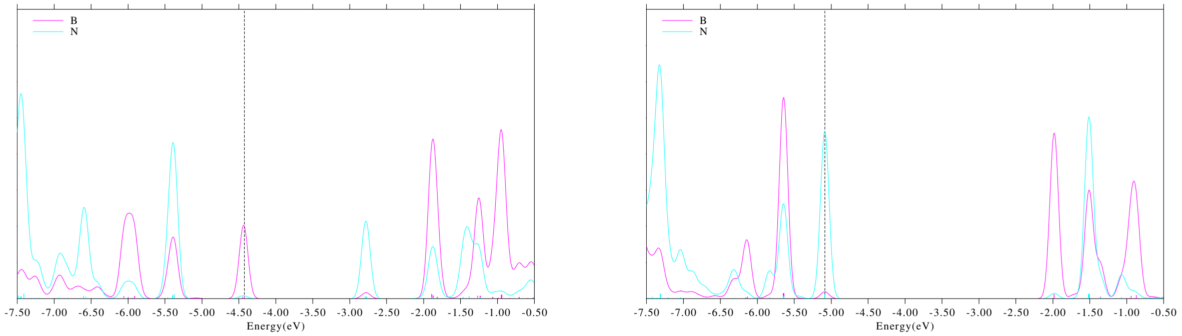

Table 1: Average π Mulliken populations for central ring. The geometry was optimized at HSE06/MINI level of calculation. Electron densities obtained according to the basis set specified in the corresponding row. All values in au and multiplied by 1000.

Molecule name	Basis set	Atom π Mulliken population		
		C	B	N
C_{84}	6-31G	1002		
HBC	6-31G	1004		
$C_{84}-B_3N_3$	6-31G		504	1497
$HBC-B_3N_3$	6-31G		474	1529
$BN13\times13-C_{84}-B_3N_3$	REF		516	1379
$BN13\times13-HBC-B_3N_3$	REF		513	1459
$BN13\times13-C_{84}-B_3N_3$	6-31G		473	1411
$BN13\times13-HBC-B_3N_3$	6-31G		479	1526
$BN13\times13-C_{84}-B_3N_3$	6-31G*		502	1384
$BN13\times13-HBC-B_3N_3$	6-31G*		507	1501

2 References

References

1. Dovesi, R.; Orlando, R.; Erba, A.; Zicovich-Wilson, C. M.; Civalleri, B.; Casassa, S.; Maschio, L.; Ferrabone, M.; De La Pierre, M.; D'Arco, P.; Noël, Y.; Causà, M.; Rérat, M.; Kirtman, B. *Int. J. Quantum Chem.* **2014**, *114*, 1287–1317.

2. Lu, T.; Chen, F. *J. Comput. Chem.* **2012**, *33*, 580–592.